Electronic Supplementary Material (ESI) for ChemComm.

Supplementary Information

Integrating fluorinated photoactive chromophore into metal-organic frameworks for selective trifluoroethylation of styrenes

Leixin Hou, Xu Jing*, Huilin Huang and Chunying Duan

State Key Laboratory of Fine Chemicals, Zhang Dayu College of Chemistry, Dalian University of Technology, Dalian, 116024, P. R. China

Corresponding Authors

* E-mail: xjing@dlut.edu.cn

Contents

1. General Materials and Methods
2. Experimental Section
3. Single Crystal Analysis of Zn-TFBD
4. Characterization of Zn-TFBD and Zn-TPBD
5. Photocatalytic Trifluoroethylation Details Mediated by Zn-MOFs
6. NMR Spectra of Ligands
7. References

1. General Materials and Methods

All starting chemicals and reagents were commercially available and used without further purification unless specifically mentioned. Powder X-ray diffraction (PXRD) measurements were obtained on a Rigaku Smart Lab XRD instrument with a sealed Cu tube (λ = 1.54178 Å). Thermogravimetric (TG) analyses were performed from 20 to 800 ℃ at a heating rate of 10 ℃ min^{-1} and a N_2 flow rate of 50 mL min^{-1}. Fourier transform infrared (FT-IR) spectra were collected in the range of 400–3500 cm^{-1} as KBr pellets on Thermo Fisher-6700. Raman spectra were collected on a Lab Raman HR Evolution at excitation wavelength of 633 nm in a scan range from 500 to 3500 cm^{-1} on powdered samples on air. Nitrogen sorption isotherms were recorded on a Quantachrome Autosorb-iQ at 77 K within a pressure range from P/P_0 = 0.001–0.99. The specific surface areas were evaluated by the Brunauer-Emmett-Teller (BET) method. Scanning electron microscopy (SEM) images were recorded with an HITACHI UHR FE-SEM SU8220 scanning electron microscope equipped with a field emission gun operated at 3–5 kV. The solid UV-vis spectra were recorded on a Hitachi U-4100 UV-vis-NIR spectrophotometer. Fluorescence and time-dependent luminescence decays spectra were collected on a FLS920 full-featured fluorescence spectrometer. Electron spin resonance (ESR) signals were collected on a Bruker ELEXSYS E500 at room temperature under 500 W xenon lamp (λ > 380 nm) irradiation. The electrochemical measurements were conducted in a conventional three-electrode cell on a CHI-760E electrochemical workstation (Shanghai Chenhua Instrument Co., Ltd, China). ^{1}H and ^{19}F spectra were recorded in the designated solvents on Varian DLG 400 M spectrometer with chemical shift in ppm.

2. Experimental Section

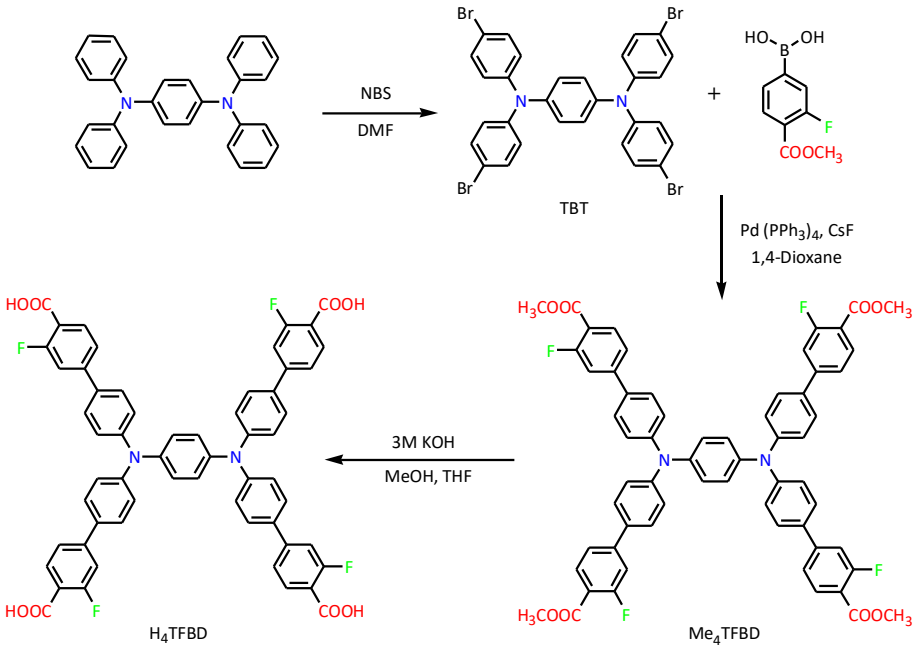

Scheme S1. Synthesis route of H_4TFBD

N^1,N^1,N^4,N^4-tetrakis(4-bromophenyl)benzene-1,4-diamine (TBT)

Compound TBT was synthesized according to literature methods without modification and characterized by ^{1}H NMR.[S1]

^{1}H NMR (600 MHz, $CDCl_3$) δ 7.35 (d, J = 8.0 Hz, 8H), 6.94 (s, 12H).

Tetramethyl-N^1,N^1,N^4,N^4-tetrakis[3-fluoro-(1,1'-biphenyl)-4-carboxylate]-1,4-benzene diamine (Me_4TFBD)

As shown in Scheme S1, compound TBT (3.35 g, 4.6 mmol), 3-fluoro-4-(methoxycar-bonyl)-phenylboronic acid (5.5 g, 27.8 mmol), CsF (8.0 g, 52.6 mmol) and $Pd(PPh_3)_4$ (0.45g) were charged in a 500 mL three-neck round bottom flask equipped with a magnetic stir bar. Dioxane (extra dry, 240 mL) was added, and the mixture was degassed by sparring with argon for 30 min. The flask was capped and heated to 90 °C under argon atmosphere for 72 h. After cooling down to room temperature, the solvent was removed using a rotary evaporator, and the crude product was dissolved in CH_2Cl_2 (600 mL) and washed with brine (3 × 400 mL). The combined organic fractions were dried over anhydrous Na_2SO_4, the solvent was removed under vacuum, and then the solid was recrystallized from dichloromethane to afford compound Me_4TFBD as yellow solid (3.1 g, yield: 65%).

^{1}H NMR (500 MHz, $CDCl_3$) δ 7.88 (dd, *J* = 8.1, 1.6 Hz, 4H), 7.81 (dd, *J* = 11.2, 1.6 Hz, 4H), 7.53 (m, 12H), 7.24 (s, 4H), 7.16 (s, 4H), 3.94 (s, 12H).

^{19}F NMR (470 MHz, $CDCl_3$) δ -117.07 (s).

N^1,N^1,N^4,N^4-tetrakis[3-fluoro-(1,1'-biphenyl)-4-carboxylicacid]-1,4-benzene diamine (H_4TFBD)

Compound Me_4TFBD (2 g, 1.96 mmol) was dissolved in 110 mL of THF to which 110 mL of 3 M KOH and 90 mL of MeOH was added. The resulting suspension was stirred under reflux for 24 h. After cooling down to room temperature, the organic solvent was removed in vacuo. The aqueous phase was acidified with 6 M HCl until pH = 2 was reached. The precipitate was filtered, washed with 300 mL of H_2O and dried under vacuum to get H_4TFBD as yellow solid (1.63 g, yield: 86%).

^{1}H NMR (500 MHz, DMF-D7) δ 7.95 (dd, *J* = 8.0, 1.5 Hz, 4H), 7.82 (m, 8H), 7.71 (dd, *J* = 8.5, 1.4 Hz, 8H), 7.34 (d, *J* = 5.1 Hz, 8H), 7.32 (s, 4H).

^{19}F NMR (470 MHz, DMF-D7) δ -118.16 (s).

Synthesis of Zn-TFBD

$Zn(NO_3)_2 \cdot 4H_2O$ (30.0 mg, 0.112 mmol) and H_4TFBD (10.0 mg, 0.0104 mmol) were dissolved in 2 mL dimethylacetamide (DMAc) in a 8 mL glass vial by ultrasonication (10 min). MeOH (1.0 mL) was added to the clear bright yellow solution and the reaction mixture was heated to 105 °C for 48 h and subsequently cooled to room temperature with a rate of 0.1 K/min. Bright yellow crystals were collected via filtration and washed with excess DMAc to afford Zn-TFBD (Yield: 31 % based on Zn).

Synthesis of Zn-TPBD

The Zn-TPBD was synthesized according to the methods in the literature.[S2]

$Zn(NO_3)_2 \cdot 4H_2O$ (20.0 mg, 0.075 mmol) and H_4TPBD (10.0 mg, 0.0111 mmol) were dissolved in 2 mL dimethylacetamide (DMAc) in a 8 mL glass vial by ultrasonication (10 min). MeOH (0.5 mL) was added to the clear bright yellow solution and the reaction mixture was heated to 105 °C for 48 h and subsequently cooled to room temperature with a rate of 0.1 K/min. Bright yellow crystals were collected via filtration and washed with excess DMAc to afford Zn-TPBD (Yield: 45 % based on Zn).

Measurements of proton conductivity (σ) for Zn-MOFs

Electrochemical impedance spectra (EIS) data of the Zn-MOFs samples were measured under 99% relative humidity (RH) at various temperatures in order to quantitatively estimate the proton conductivities of Zn-MOFs at various temperatures. The CHI760E electrochemical workstation was used over a frequency range from 1 Hz to 1 MHz with an oscillating voltage of 50 mV by a quasi-four probe method. The measurements were performed using the pellet, which was obtained by pressing Zn-TFBD and Zn-TPBD microcrystalline powder at 5 MPa for 3 min. For measuring proton conductivities of the pellet at various temperatures, the measurements were conducted during a heating process every 10 °C from 20 to 90 °C. The proton conductivity (σ) of Zn-MOFs pellet at each temperature was calculated by using the following equation

$$\sigma = \mathrm{L}/(RS)$$

where σ is proton conductivity ($S \cdot cm^{-1}$), L is the thickness of the pellet (cm), R is the resistance (Ω), and S is the superficial area of the pellet (cm^2). The resistance values were obtained from extrapolate impedance plot by using ZSimpWin software.

Afterwards, the following Arrhenius equation was used to evaluate the activation energy (E_a) for proton transport within Zn-MOFs material

$$\ln(\sigma T) = \ln(\sigma_0) - \frac{E_a}{k_B T}$$

where σ_0 is the pre-exponential factor determined experimentally, E_a (eV) is the transport activation energy, T is the temperature, and k_B is Boltzmann constant, which is 8.617×10^{-5} eV K^{-1}.

For measuring proton conductivities under various RH, the temperature was set at 20 °C, and the saturated aqueous solution of K_2CO_3, NaBr, KCl, or KNO_3 were used to replace the deionized water loaded within the sealed glass chamber to obtain the RH of 45, 65, 85 or 95% in the headspace measured by a humidity sensor, respectively. For each RH, the Zn-MOFs pellet was also placed in the headspace for 24 h and equilibrated for 30 min before collecting the EIS data. The proton conductivity (σ) of both Zn-MOFs pellet at each RH was calculated and summarized in Table S4.

General Procedure for Photocatalytic Trifluoroethylation of 4-methoxystyrene

4-methoxystyrene (0.1 mmol), 2-Iodo-1,1,1-trifluoroethane (0.3 mmol), *N,N*-Diisopropylethylamine (0.3 mmol) and Zn-TFBD catalyst (0.005 mmol) were mixed and dissolved in 2 mL acetonitrile and 500 μL water in an oven-dried 8 mL quartz glass tube with a magnetic stir bar. The mixture was irradiated with a 455 nm LED at room temperature under Ar atmosphere for 24 h with stirring. Once reaction completed, the reaction mixture was cooled to room temperature. 2-fluorotoluene was added as an internal standard. The reaction mixture was diluted with CD_3CN, and the ^{19}F NMR spectrum was measured. The yield of hydroxytrifluoroethyl product (**I**, 86% yield, δ -66.15 (s) ppm)[S3] and the yield of side-product (**II**, 7% yield, δ -66.38 (s) ppm,[S4] and **III**, 6% yield, δ -66.22 (s) ppm)[S5] were determined by ^{19}F NMR integration relative to the internal standard (δ -117.75 (m) ppm).[S6]

3. Single Crystal Analysis of Zn-TFBD

Single crystal structures of Zn-TFBD was measured on a Bruker SMART APEX CCD diffractometer with Mo-Kα radiation (λ = 0.71073 Å) using the SMART and SAINT programs.[S7,S8] Absorption correction was performed by multi-scan method implemented in SADABS program. The structure was solved by direct methods and refined using SHELXL-97 software with Olex 2 (full-matrix least-squares on F^2).[S9] Anisotropic thermal parameters were applied to all non-hydrogen atoms. The disordered solvent molecules were treated as diffuse using the SQUEEZE procedure implemented in PLATON. These data can be obtained free of charge from the CCDC *via* www.ccdc.cam.ac.uk/data_request/cif. Crystal data and refinement details are shown in Tables S1.

Table S1. Crystal data and structure refinement of Zn-TFBD.

Compound	Zn-TFBD
Empirical formula	$C_{68}H_{50}F_4N_2O_{10}Zn_2$
Formula weight (g mol^{-1})	1261.84
Temperature (K)	200.0
Crystal system	monoclinic
Space group	$P2_1/c$
a (Å)	21.6596(10)
b (Å)	10.1234(5)
c (Å)	15.4018(7)
α (deg)	90
β (deg)	98.6440(10)
γ (deg)	90
Volume (Å^3)	3338.8(3)
Z	2
ρ_{calc} (g·cm^{-3})	1.255
Absorption Coefficient (mm^{-1})	0.785
F(000)	1296.0
Crystal size (mm^3)	0.30 × 0.33 × 0.1 mm
Radiation	MoKα (λ = 0.71073)
2θ range for data collection (deg)	4.45 to 50.124
Index ranges	-25 ≤ h ≤ 21, -12 ≤ k ≤ 12, -18 ≤ l ≤ 18
Reflections collected	25592
Independent reflections	5889 [R_{int} = 0.0359, R_{sigma} = 0.0364]
Data/restraints/parameters	5889/2/391
Goodness-of-fit on F^2	1.755
Final R indexes [I>=2σ (I)]	R_1 = 0.0712, wR_2 = 0.2308
Final R indexes [all data]	R_1 = 0.0863, wR_2 = 0.2377
Largest diff. peak/hole / e Å^{-3}	2.33/-0.78
CCDC number	2181503

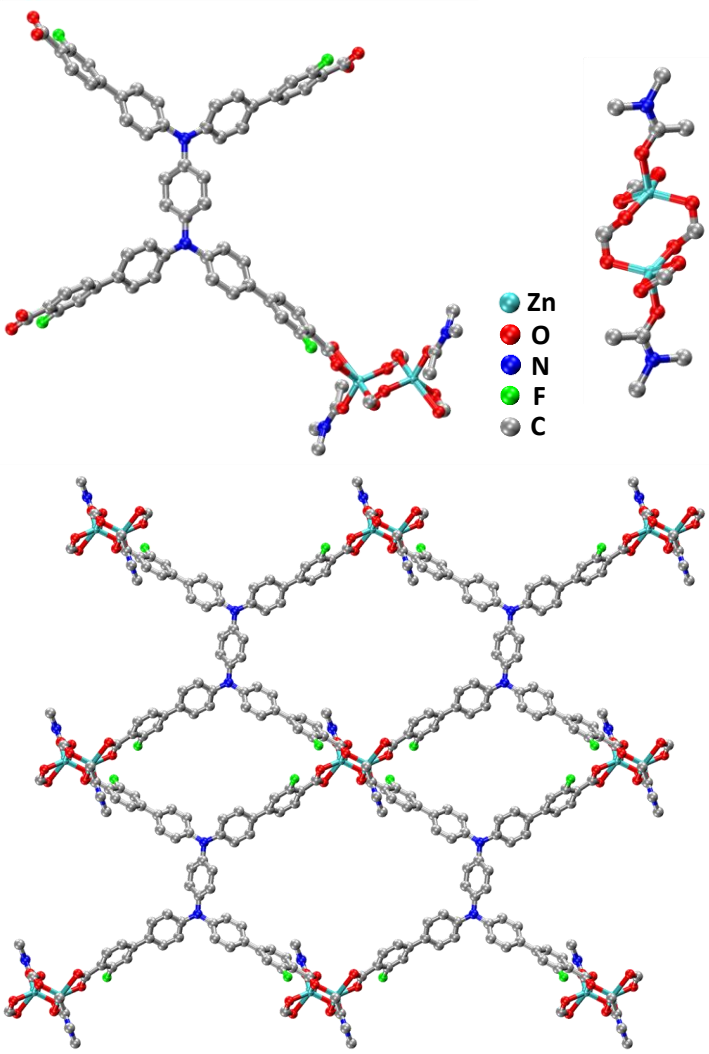

Figure S1. A section of the crystal structure of Zn-TFBD and the corresponding secondary building unit (SBU, top); Assembly of the linker TFBD and the SBU in Zn-TFBD (bottom). Displacement ellipsoids are given at the 50% probability level. Hydogen atoms have been removed, for reasons of clarity. Cyan, red, blue, green and silver spheres correspond to zinc, oxygen, nitrogen, fluorine and carbon respectively.

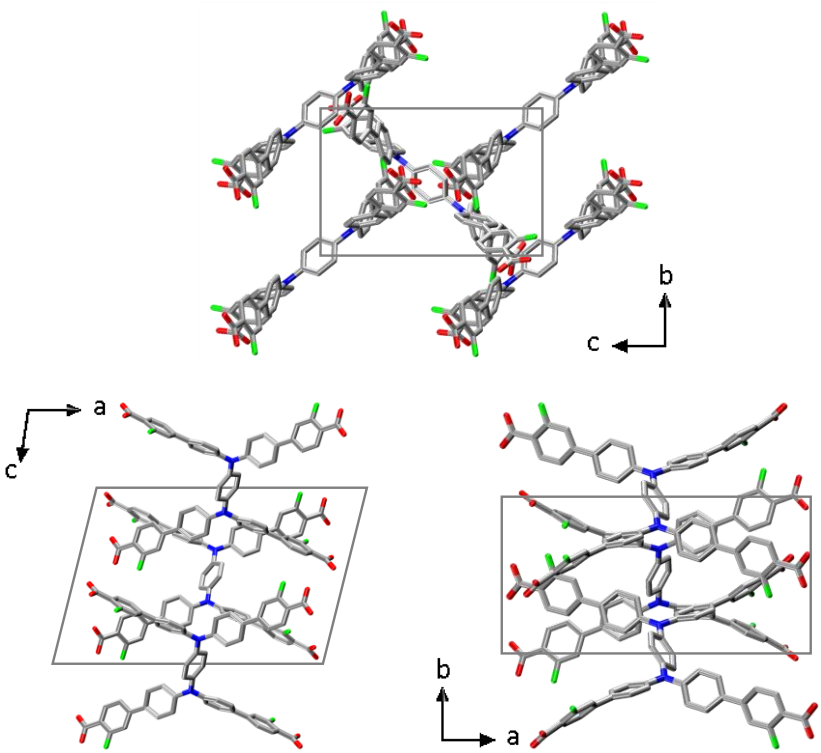

Figure S2. The packing of Me_4TFBD in Zn-TFBD. The metallic SBU has been removed due to clarity reasons. The compound shows a Herringbone type arrangement (top) with slipped, coplanar stacking along the crystallographic *b* and *c*-axis (bottom).

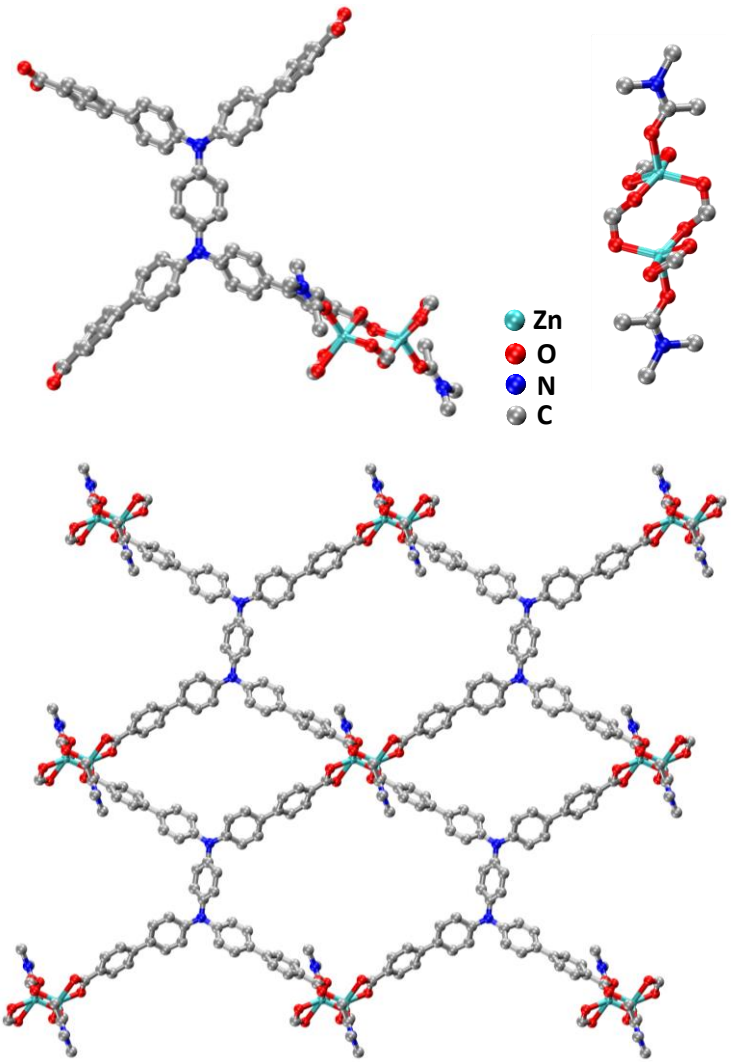

Figure S3. A section of the crystal structure of Zn-TPBD and the corresponding secondary building unit (SBU, top); Assembly of the linker TPBD and the SBU in Zn-TPBD (bottom). Displacement ellipsoids are given at the 50% probability level. Hydogen atoms have been removed, for reasons of clarity. Cyan, red, blue and silver spheres correspond to zinc, oxygen, nitrogen and carbon respectively.

4. Characterization of Zn-TFBD and Zn-TPBD

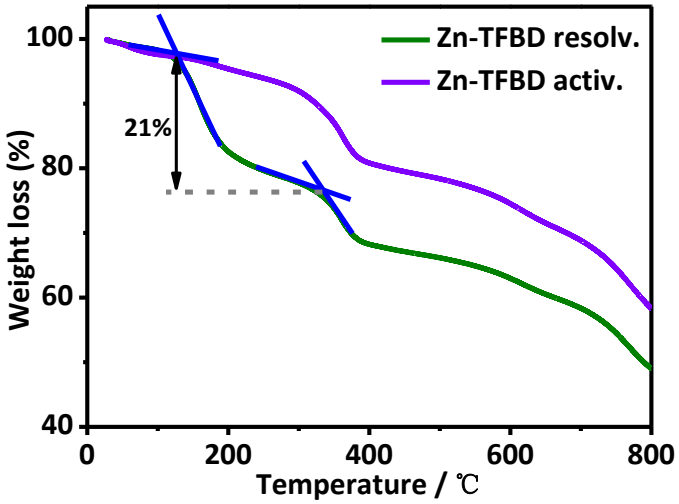

Figure S4. TGA curves of desolvated and activated samples of Zn-TFBD.

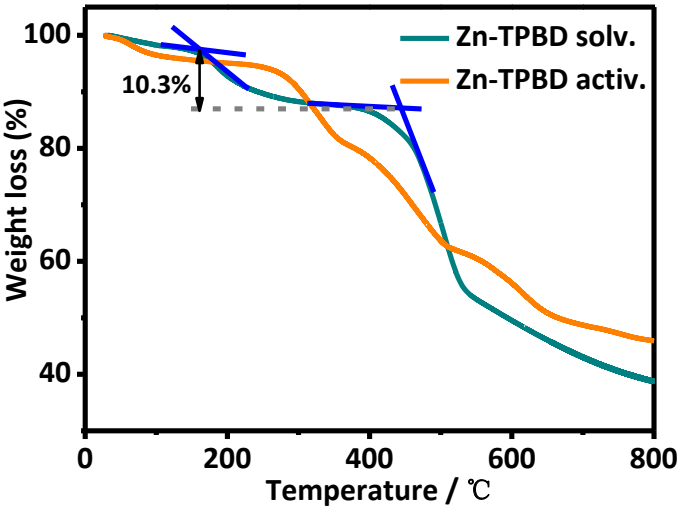

Figure S5. TGA curves of desolvated and activated samples of Zn-TPBD.

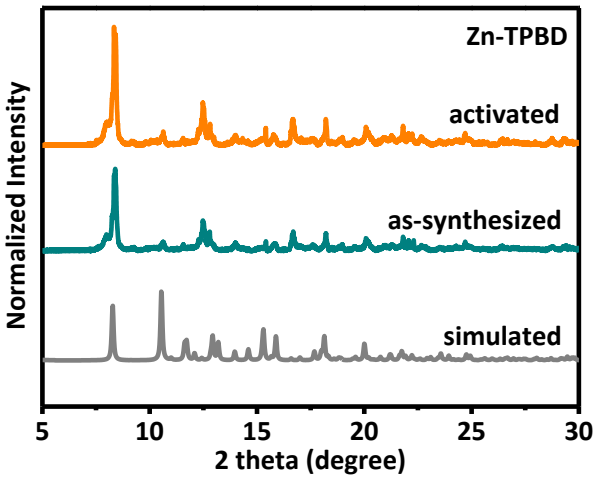

Figure S6. PXRD patterns of the as-synthesized and supercritical CO_2 activated Zn-TPBD.

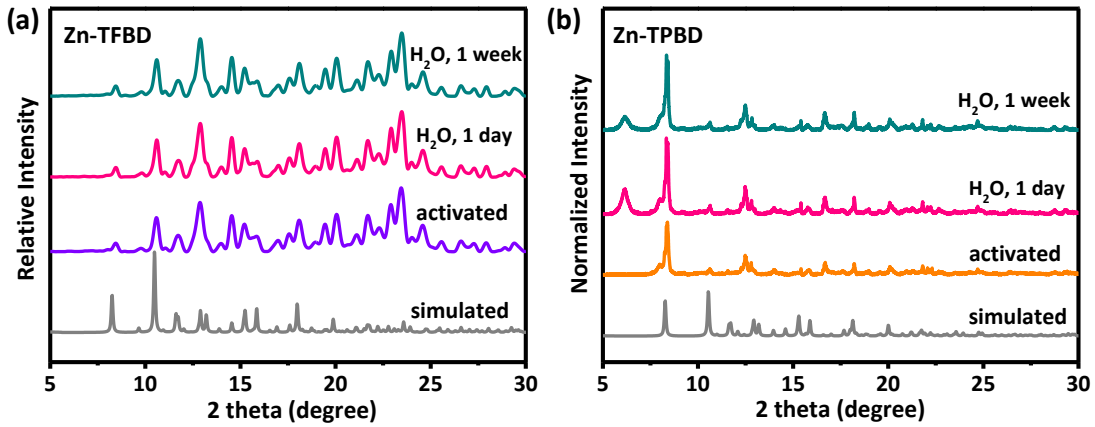

Figure S7. PXRD patterns of (a) Zn-TFBD and (b) Zn-TPBD after being treated in water.

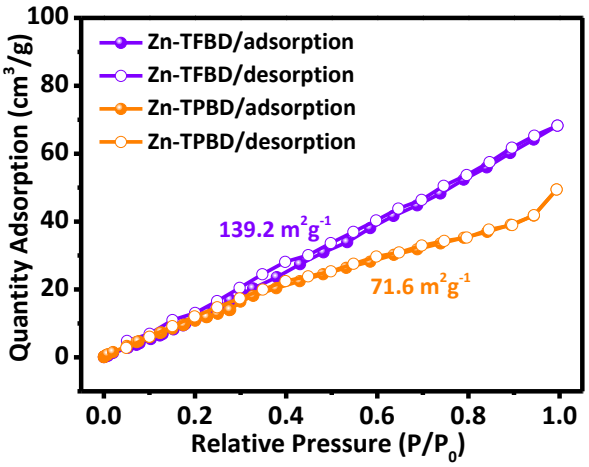

Figure S8. N_2 adsorption and desorption isotherm of the Zn-TFBD and Zn-TPBD measured at 77 K.

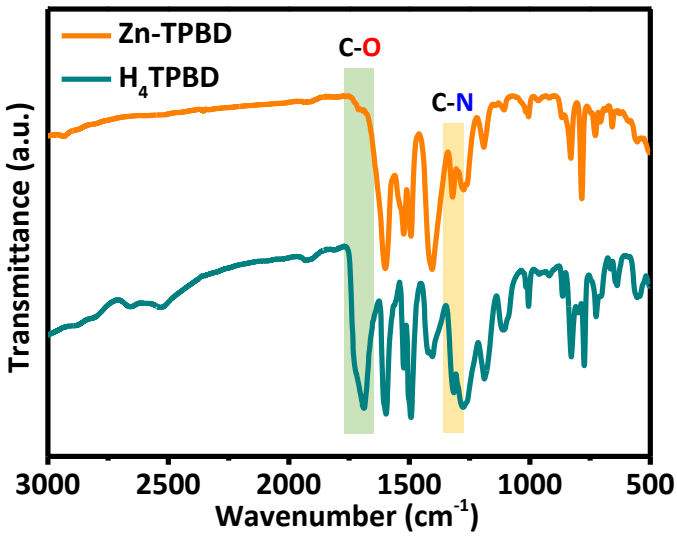

Figure S9. FT-IR spectra of H_4TPBD and Zn-TPBD.

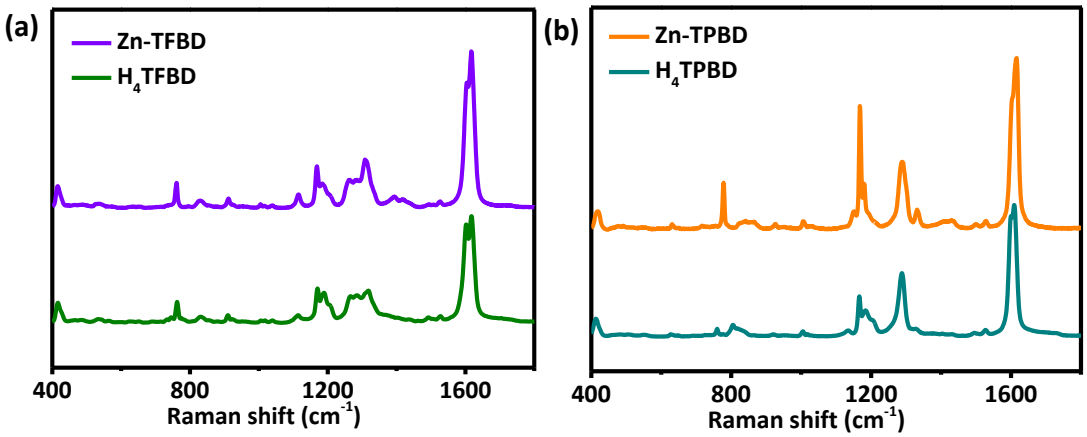

Figure S10. (a) Raman spectra of H_4TFBD and Zn-TFBD. (b) Raman spectra of H_4TPBD and Zn-TPBD.

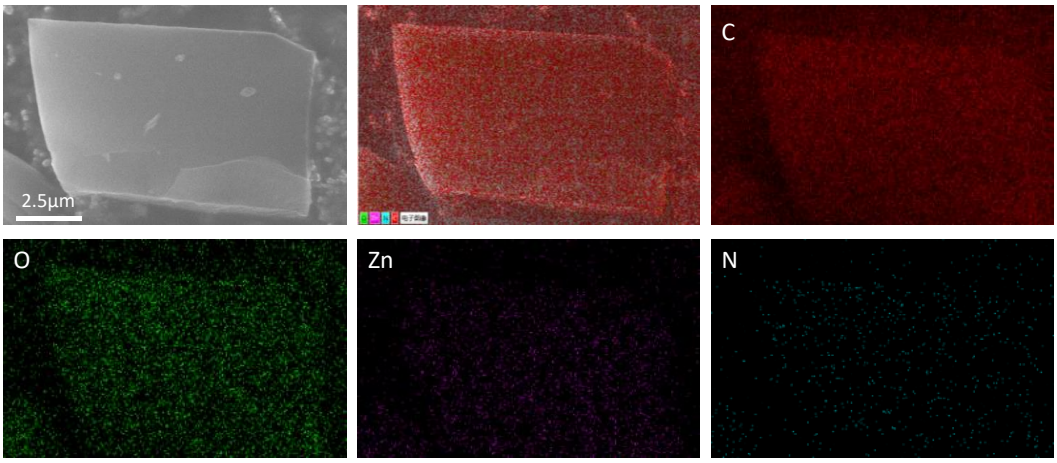

Figure S11. SEM and EDS mapping images of Zn-TPBD.

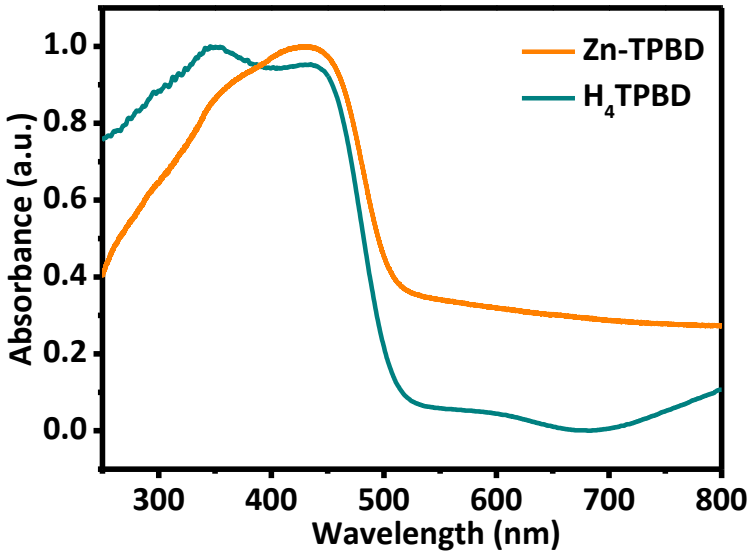

Figure S12. Solid state UV-Vis absorption spectra of H_4TPBD and Zn-TPBD.

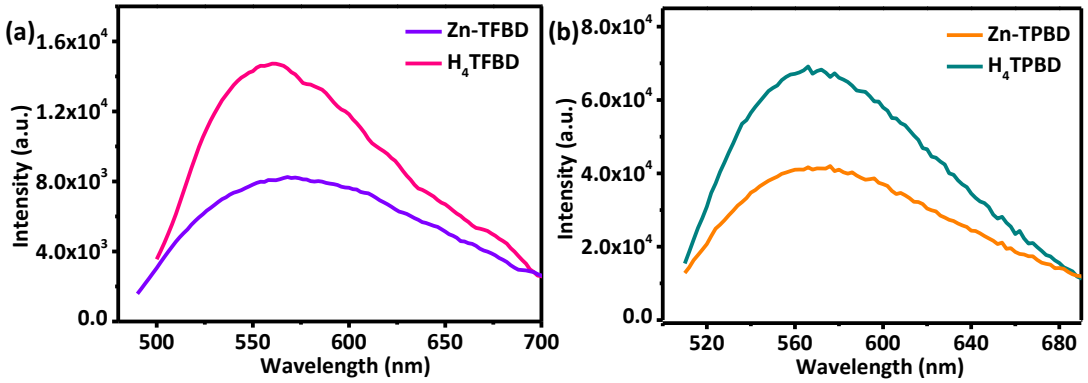

Figure S13. (a) Solid state emission spectra of H_4TFBD and Zn-TFBD. (b) Solid state emission spectra of H_4TPBD and Zn-TPBD.

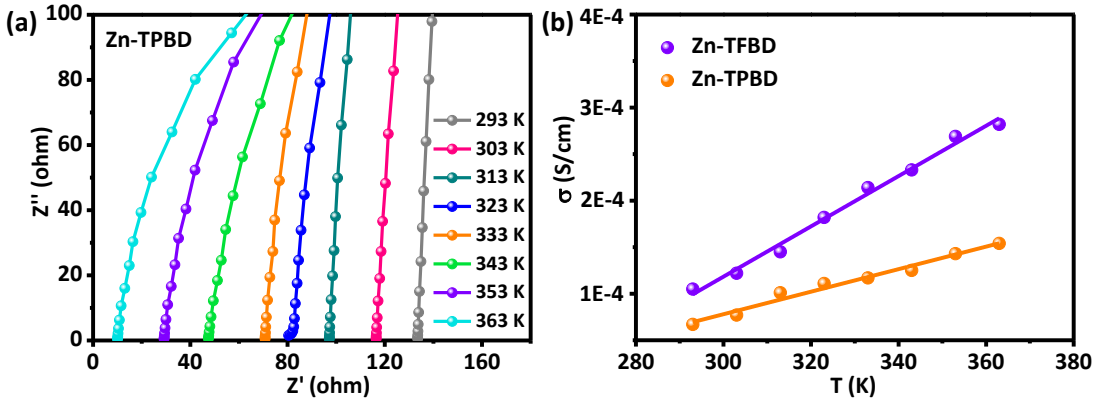

Figure S14. (a) Nyquist plots of Zn-TPBD measured under 99% RH. (b) Plots of σ vs temperature (K) for Zn-TFBD and Zn-TPBD.

Table S2. Proton conductivities of Zn-TPBD and Zn-TFBD measured under at 99% RH and different temperatures.

Temperature (K)	Zn-TPBD Conductivity (S cm^{-1})	Zn-TFBD Conductivity (S cm^{-1})
293	6.7×10^{-5}	1.05×10^{-4}
303	7.7×10^{-5}	1.22×10^{-4}
313	1.01×10^{-4}	1.45×10^{-4}
323	1.11×10^{-4}	1.82×10^{-4}
333	1.17×10^{-4}	2.14×10^{-4}
343	1.25×10^{-4}	2.33×10^{-4}
353	1.43×10^{-4}	2.69×10^{-4}
363	1.54×10^{-4}	2.82×10^{-4}

Table S3. Comparison of proton conductivity for Zn-TPBD and Zn-TFBD with other proton-conducting Zn-based MOFs materials.

Compound	Conductivity/ S cm^{-1}	Experimental conditions	References
$Zn_3(L)(H_2O)_2 \cdot 2H_2O$	3.5×10^{-5}	298 K, 98% RH	S10
$[Zn_3(H_2PO_4)_6](Hbim)$	1.3×10^{-3}	Anhydrous, 120℃	S11
$[Zn(H_2PO_4)_2(TzH)_2]_n$	1.1×10^{-4}	403 K, anhydrous	S12
$[Zn(HPO_4)(H_2PO_4)_2](ImH_2)_2$	2.5×10^{-4}	403 K, anhydrous	S13
$[Zn(H_2PO_4)_2(HPO_4)](H_2dmbim)_2$	0.2×10^{-3}	463 K, anhydrous	S14
Defective $[Zn(H_2PO_4)\ HTz_2]_n$	3.16×10^{-3}	Anhydrous, 150℃	S15
$\{[ZnL(bpe)_{0.5}] \cdot 0.5(H_2bpe) \cdot 3(H_2O)\}_n$	7.29×10^{-3}	353 K, 58% RH	S16
$\{[Zn_2(1,2,4,5\text{-BTA})](4,40\text{-tmdp})_2] \cdot 5H_2O\}_n$	1.09×10^{-4}	373 K, 98% RH	S17
Zn-TPBD	1.54×10^{-4}	363 K, 99% RH	This work
Zn-TFBD	2.82×10^{-4}	363 K, 99% RH	This work

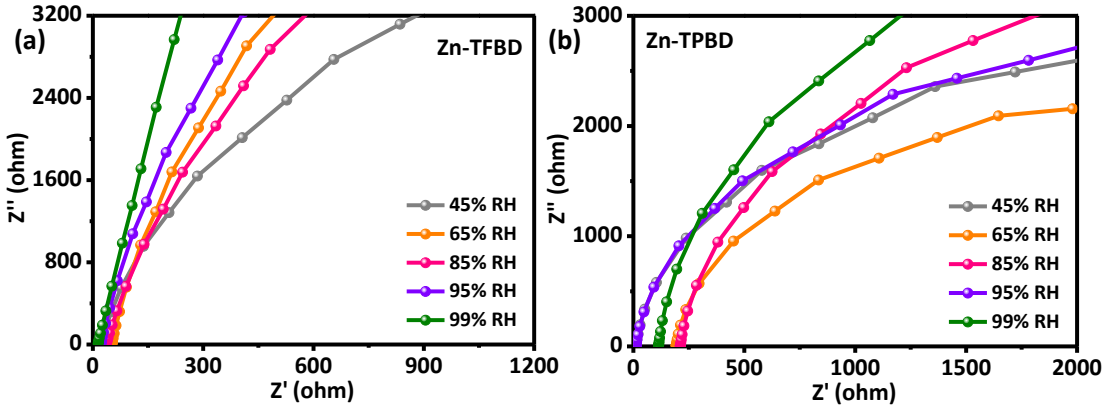

Figure S15. Nyquist plots of (a) Zn-TFBD and (b) Zn-TPBD measured under various RH levels at 293 K.

Table S4. Conductivity of Zn-TPBD and Zn-TFBD recorded at 293 K and different RH levels.

Relative Humidity (%)	Zn-TPBD Conductivity (S cm^{-1})	Zn-TFBD Conductivity (S cm^{-1})
45	2.4×10^{-6}	3.7×10^{-6}
65	3.6×10^{-6}	8.3×10^{-6}
85	4×10^{-6}	9.6×10^{-6}
95	6.2×10^{-6}	1.1×10^{-5}
99	1×10^{-5}	1.5×10^{-5}

5. Photocatalytic Trifluoroethylation Details Mediated by Zn-TFBD

Table S5. Optimization reaction conditions for photocatalytic trifluoroethylation of 4-methoxystyrene.

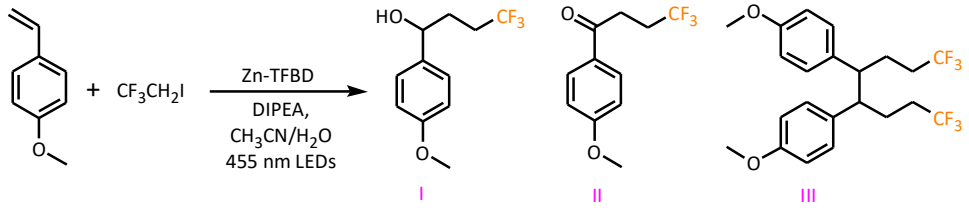

Entry	Difference from the standard condition[a]	Con (%)	Yield I/II/III (%)[b]
1	None	98	86/7/5
2	No Zn-TFBD	<1	<1
3	No light	<1	<1
4	No DIPEA	<1	<1
5	Zn-TPBD instead of Zn-TFBD	88	58/18/12
6	$Zn(NO_3)_2$ instead of Zn-TFBD	<1	<1
7	H_4TFBD instead of Zn-TFBD	<1	<1
8	H_4TPBD instead of Zn-TFBD	<1	<1
9	$Zn(NO_3)_2$/H_4TFBD instead of Zn-TFBD	<1	<1
10	$Zn(NO_3)_2$/H_4TPBD instead of Zn-TFBD	<1	<1
11	Air instead of Ar	<1	<1
12	No H_2O	<1	<1
13	H_2O (200 μL) / CH_3CN as reaction solvent	28	12/1/5
14	H_2O (400 μL) / CH_3CN as reaction solvent	86	72/4/10

[a] Reaction conditions: 4-methoxystyrene (0.1 mmol), 2-Iodo-1,1,1-trifluoroethane (0.3 mmol), *N,N*-Diisopropylethylamine (0.3 mmol), and Zn-TFBD catalyst (0.005 mmol) in CH_3CN (2 mL) and water (500 μL) irradiated with 455 nm LED under Ar atmosphere at room temperature for 24 h. [b] Yields of fluorides are determined by ^{19}F NMR integration of reaction mixtures with an internal standard 2-fluorotoluene.

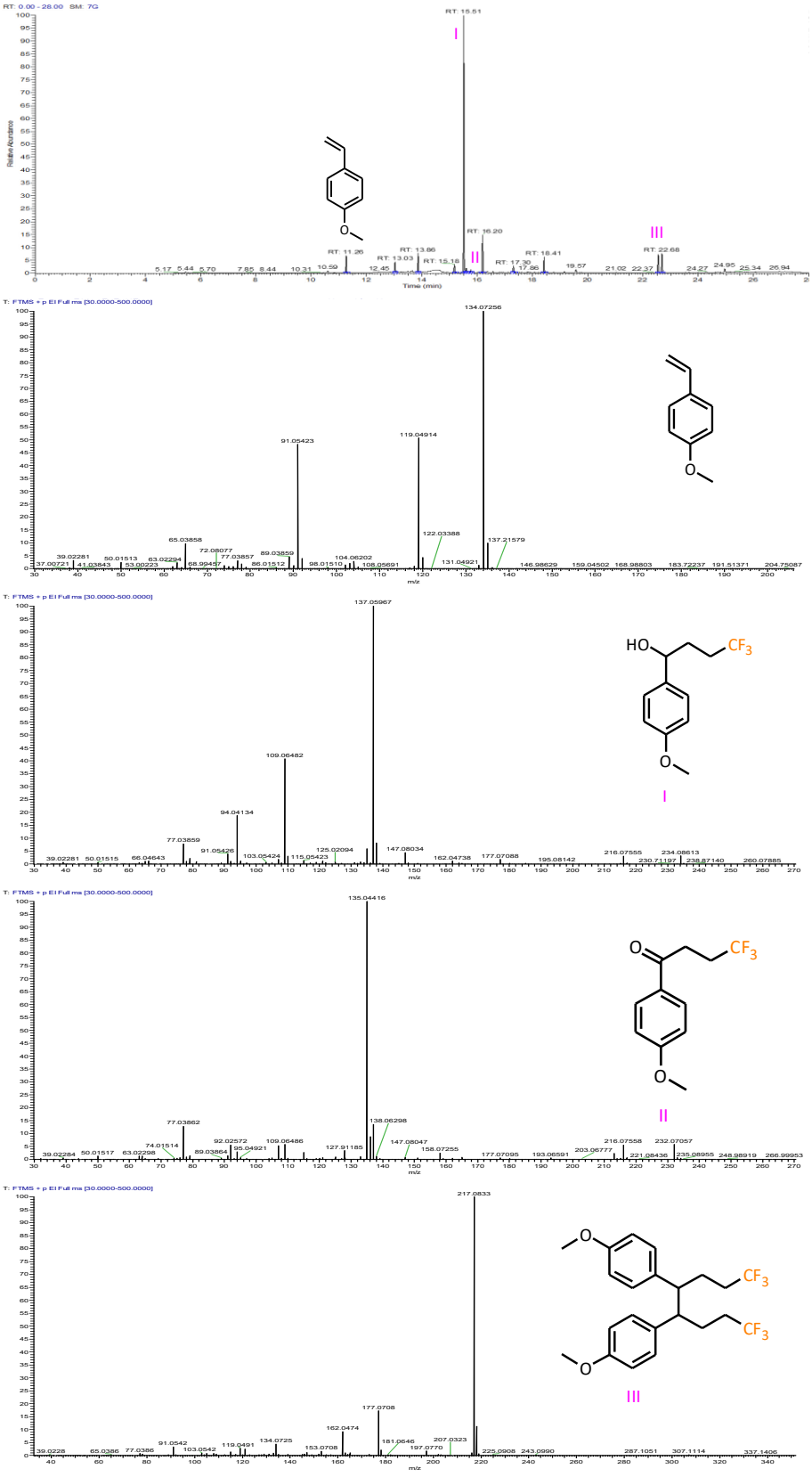

Figure S16. GC-MS of trifluoroethylation reaction of 4-methoxystyrene catalyzed by Zn-TFBD.

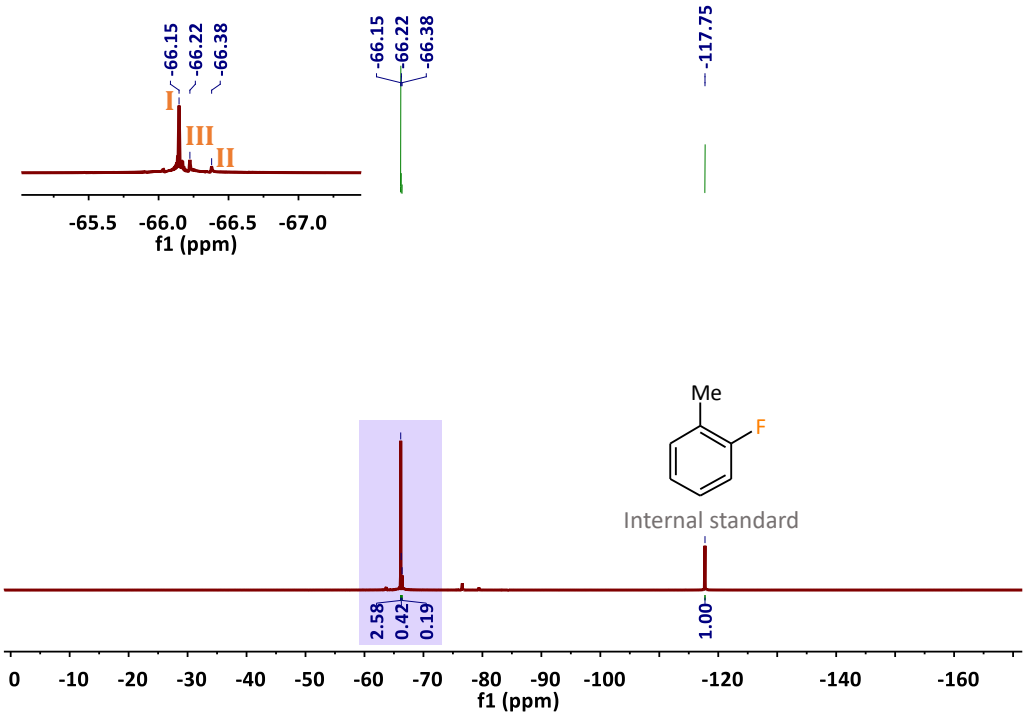

Figure S17. ^{19}F NMR spectrum of the resulting mixtures for product I, side-products II and III under photocatalytic trifluoroethylation with Zn-TFBD.

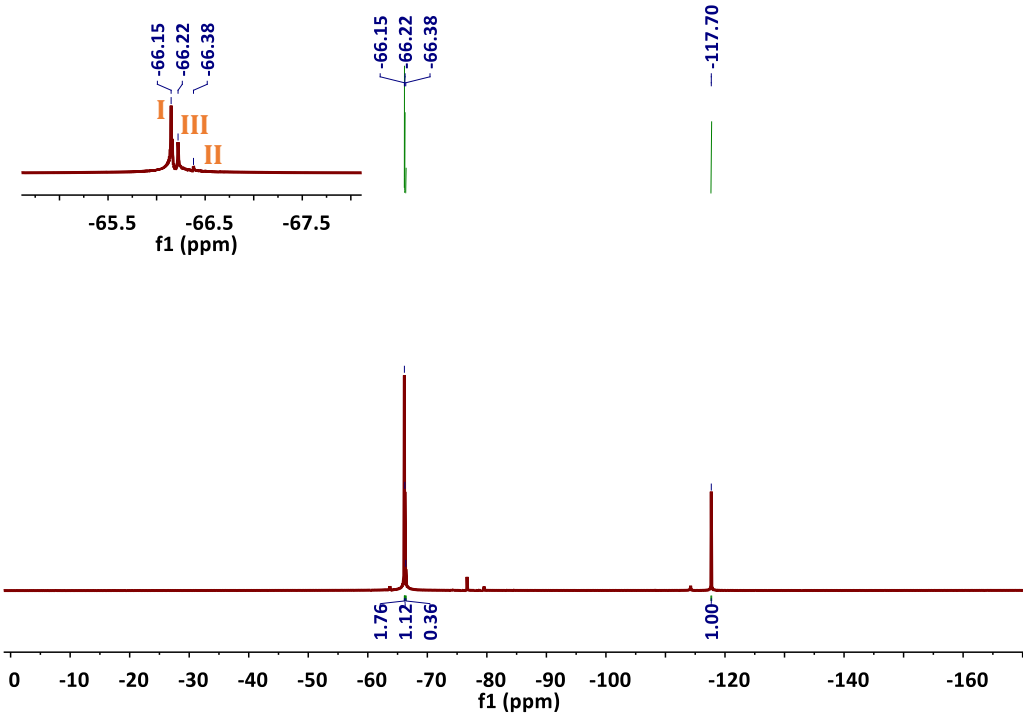

Figure S18. ^{19}F NMR spectrum of the resulting mixtures for product I, side-products II and III under photocatalytic trifluoroethylation with Zn-TPBD.

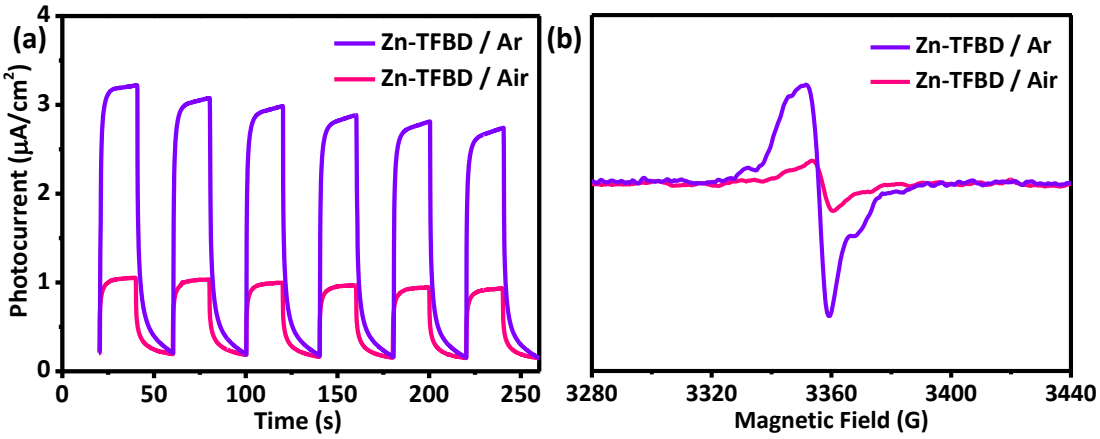

Figure S19. (a) Transient photocurrent responses and (b) ESR spectra of Zn-TFBD under Air and Ar atmosphere.

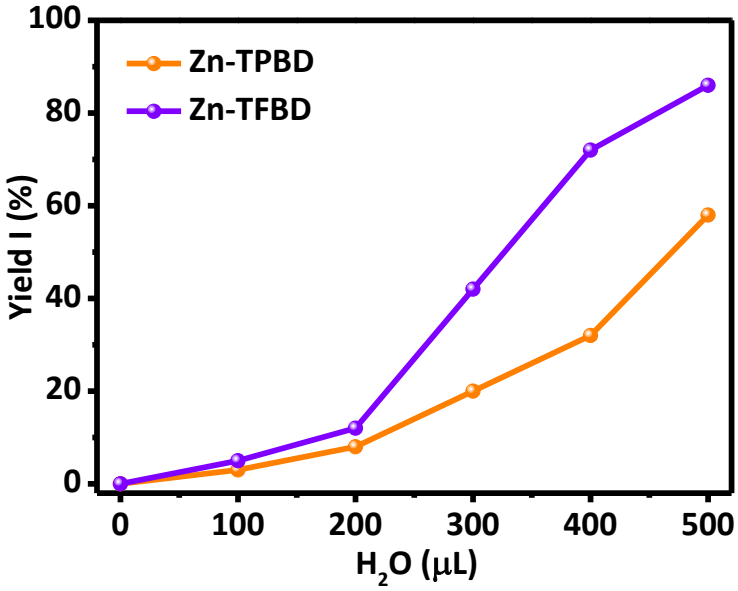

Figure S20. The effect of moisture content on hydroxytrifluoroethylation catalyzed by Zn-TFBD and Zn-TPBD under Ar atmosphere.

Solvent screening of photocatalytic trifluoroethylation with Zn-TFBD

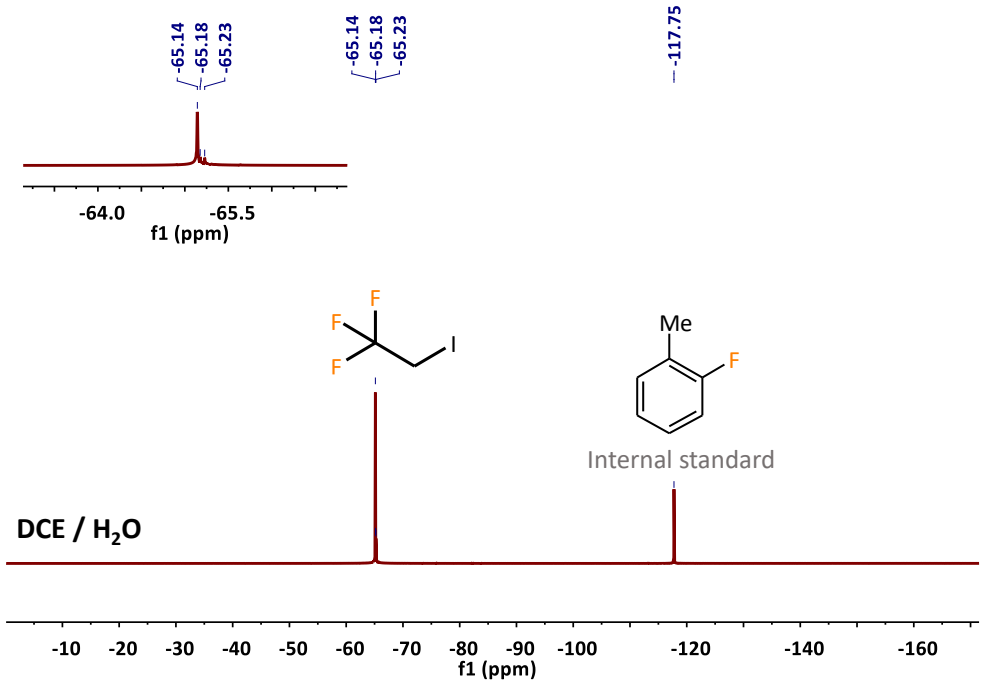

Figure S21. ^{19}F NMR spectrum of the resulting mixtures under photocatalytic trifluoroethylation with Zn-TFBD in the presence of dichloroethane and water. No desired product was found in the reaction mixture.

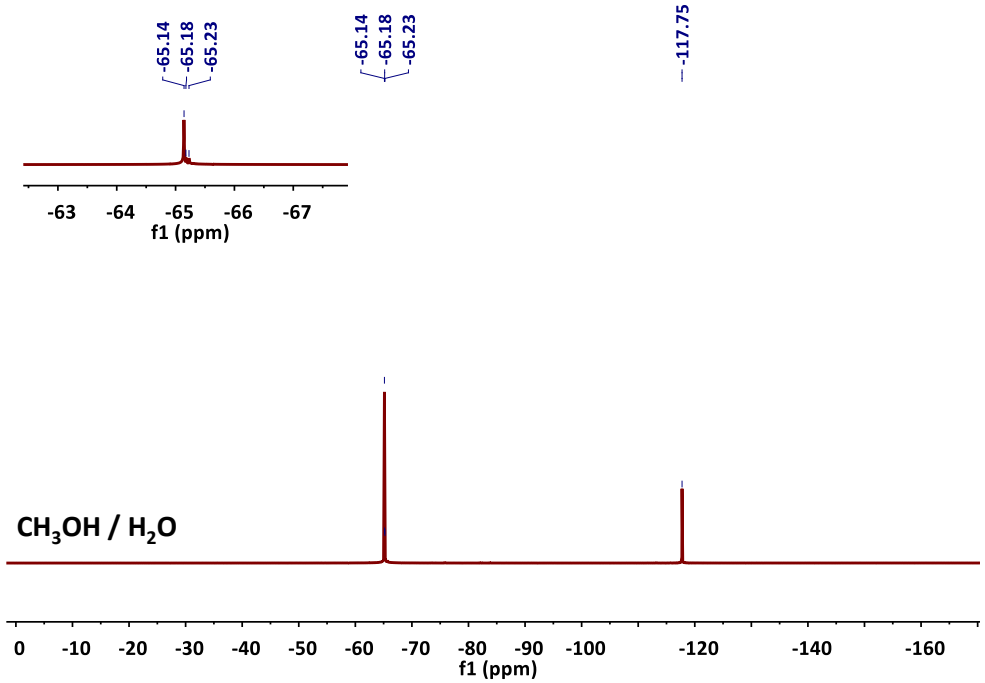

Figure S22. ^{19}F NMR spectrum of the resulting mixtures under photocatalytic trifluoroethylation with Zn-TFBD in the presence of methanol and water.

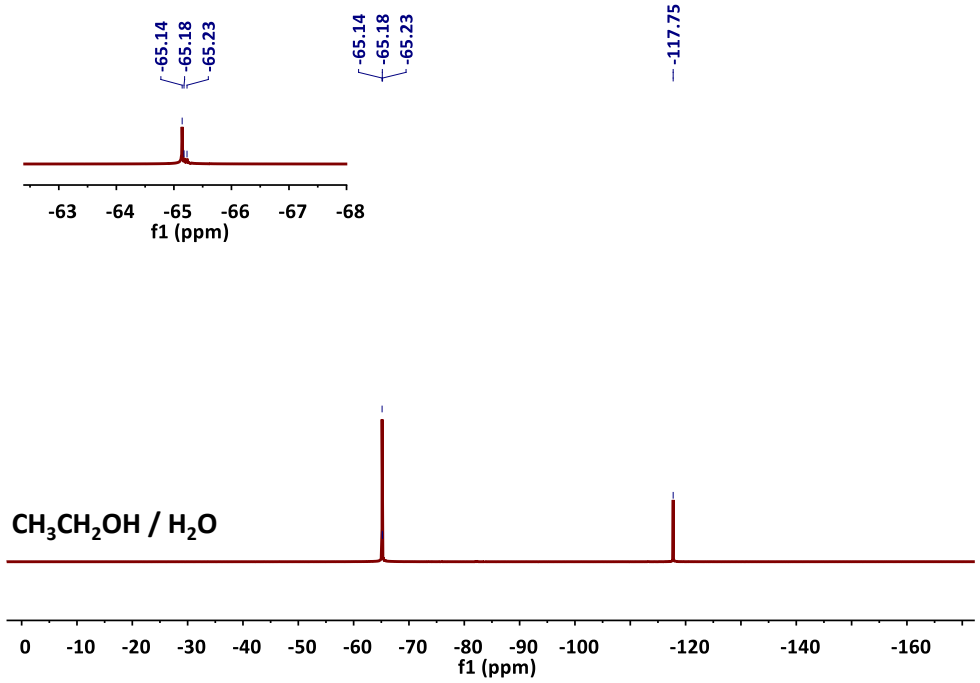

Figure S23. ^{19}F NMR spectrum of the resulting mixtures under photocatalytic trifluoroethylation with Zn-TFBD in the presence of ethanol and water.

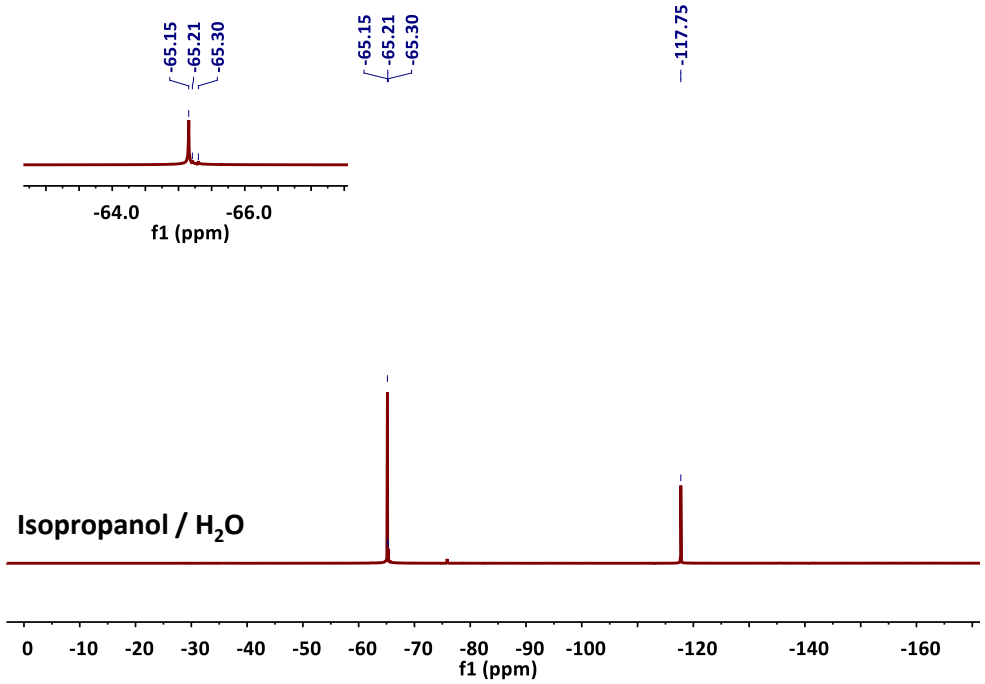

Figure S24. ^{19}F NMR spectrum of the resulting mixtures under photocatalytic trifluoroethylation with Zn-TFBD in the presence of isopropanol and water.

Leaching experiment and recyclability test of trifluoroethylation with Zn-TFBD

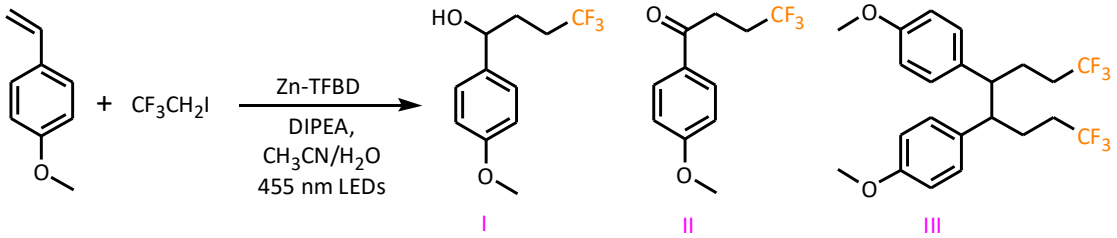

The filtrate leaching study was set up following the aforementioned general procedure using 4-methoxystyrene (0.1 mmol), 2-Iodo-1,1,1-trifluoroethane (0.3 mmol), *N,N*-Diisopropylethylamine (0.3 mmol) and Zn-TFBD catalyst (0.005 mmol) were mixed and dissolved in 2 mL acetonitrile and 500 µL water. After the addition of all components, the reaction tube was placed under 455 nm LED irradiation where it was stirred at room temperature under Ar atmosphere. Further, by separating the photocatalyst from reaction mixture by centrifugation after 6 h yielded 38 % conversion (based on ^{19}F NMR). Exposing this reaction mixture with 455 nm LED under continuous stirring for 6 h did not reveal any further conversion. The filtered photocatalyst was then transferred to the reaction tube which was irradiated with 455 nm LED, using ^{19}F NMR to monitor conversion and yield during process.

To test recyclability, the supernatant was decanted from the photocatalyst after 24 h reaction and the photocatalyst was washed with acetonitrile (3×20 mL). The washed Zn-TFBD were directly used for the next round photocatalytic trifluoroethylation of 4-methoxystyrene. The conversion and yield of products were monitored using ^{19}F NMR with 2-fluorotoluene as an internal standard.

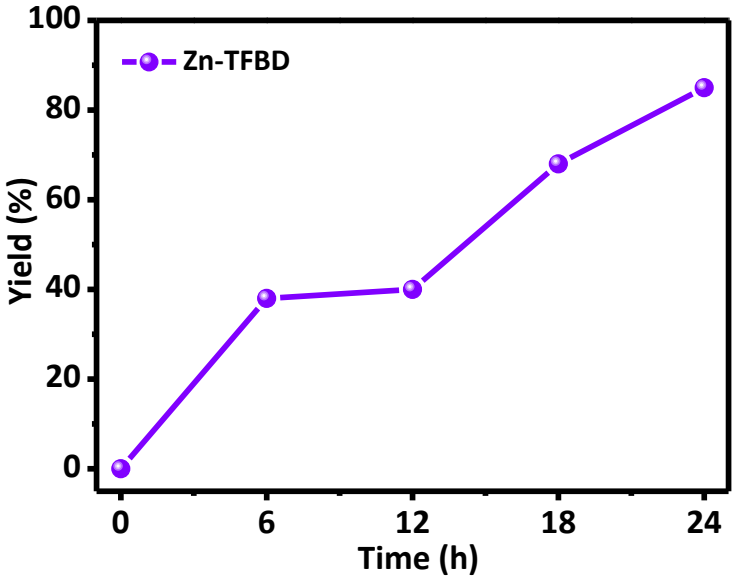

Figure S25. Catalyst filtration experiment of hydroxytrifluoroethylation catalyzed by Zn-TFBD. The photocatalyst is present in the first 0-6 h; the catalyst is separated during 6-12 h; the catalyst is recovered after 12 h.

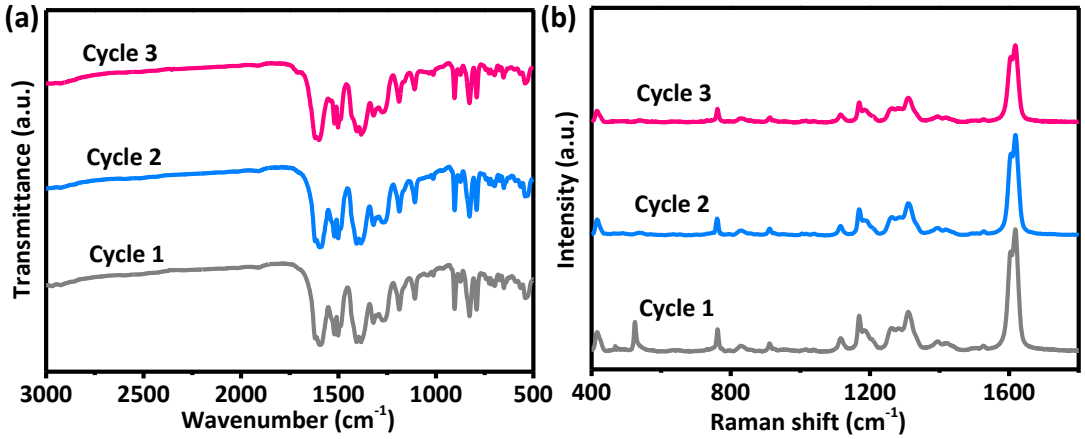

Figure S26. (a) FT-IR and (b) Raman spectra of the Zn-TFBD after three catalytic cycles of hydroxytrifluoroethylation of 4-methoxystyrene.

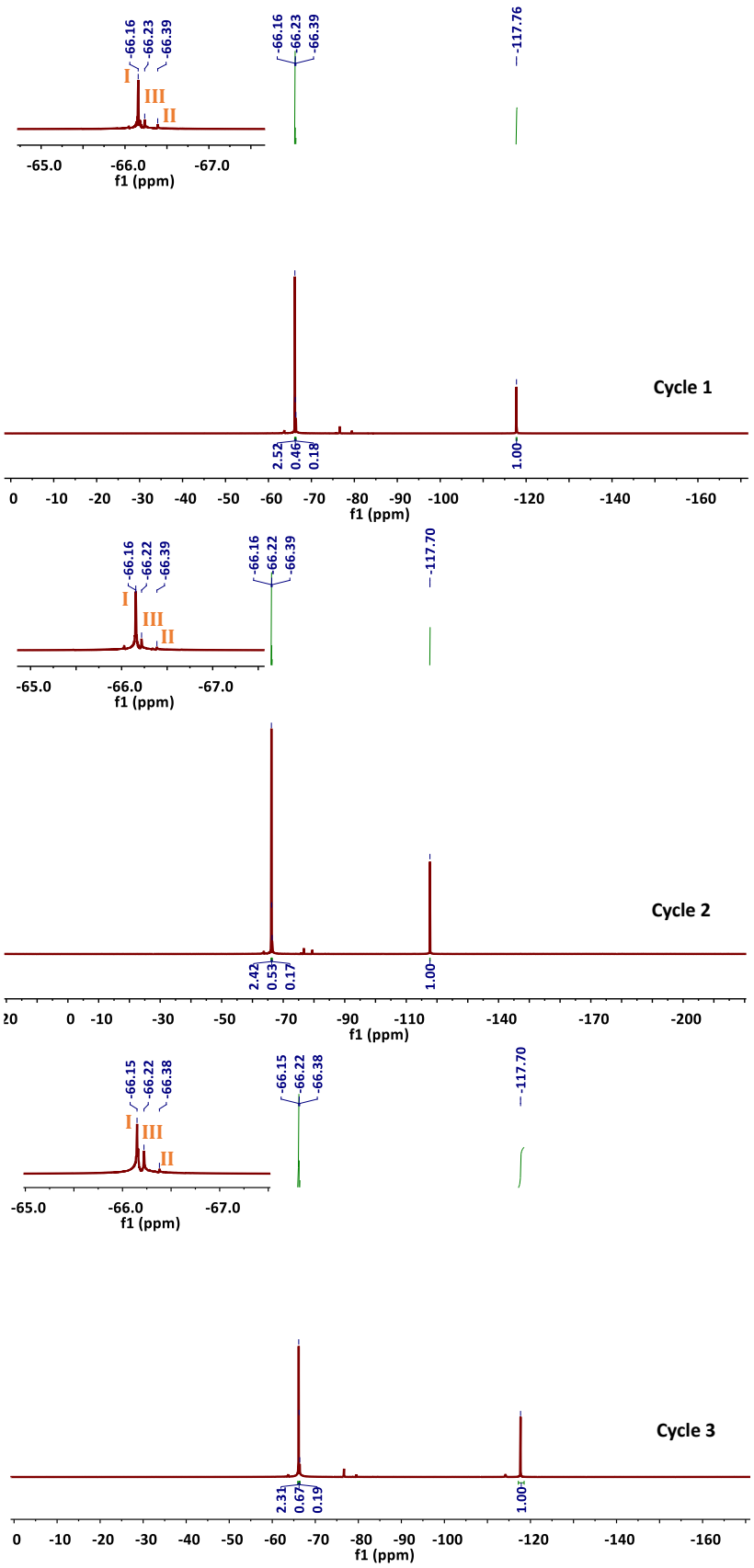

Figure S27. ^{19}F NMR spectra of hydroxytrifluoroethylation of 4-methoxystyrene catalyzed by Zn-TFBD for three cycling experiments.

6. NMR Spectra of Ligands

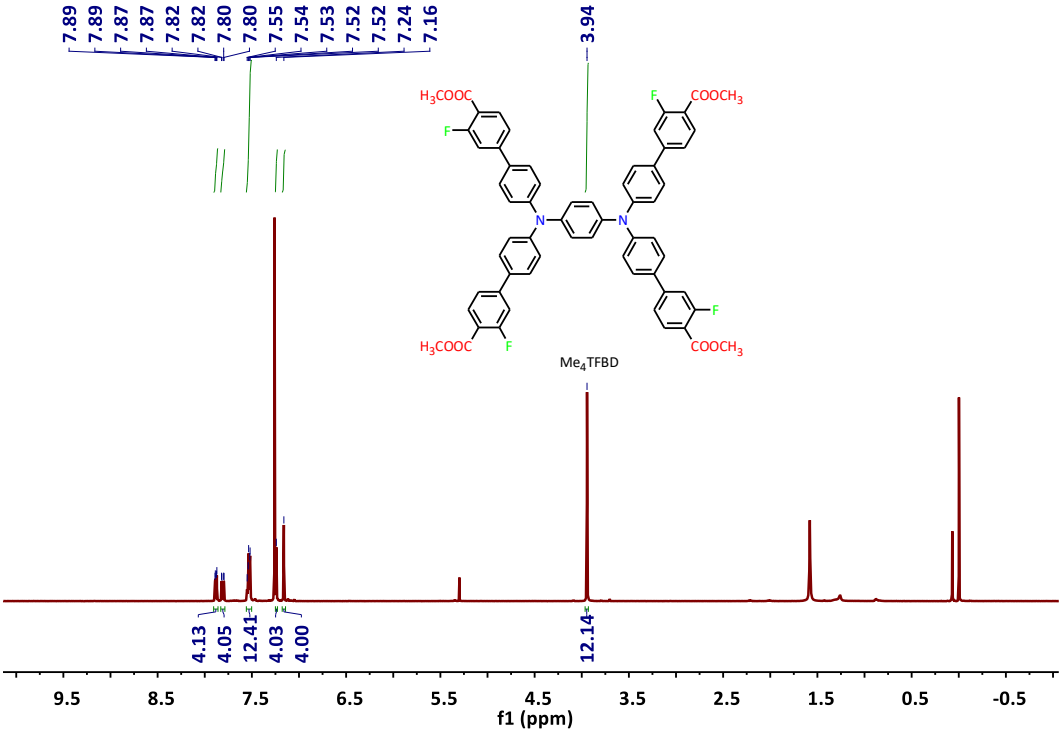

Figure S28. ^{1}H NMR (500 MHz) spectrum of Tetramethyl-N^{1},N^{1},N^{4},N^{4}-tetrakis[3-fluoro-(1,1‘-biphenyl)-4-carboxylate]-1,4-benzene diamine.

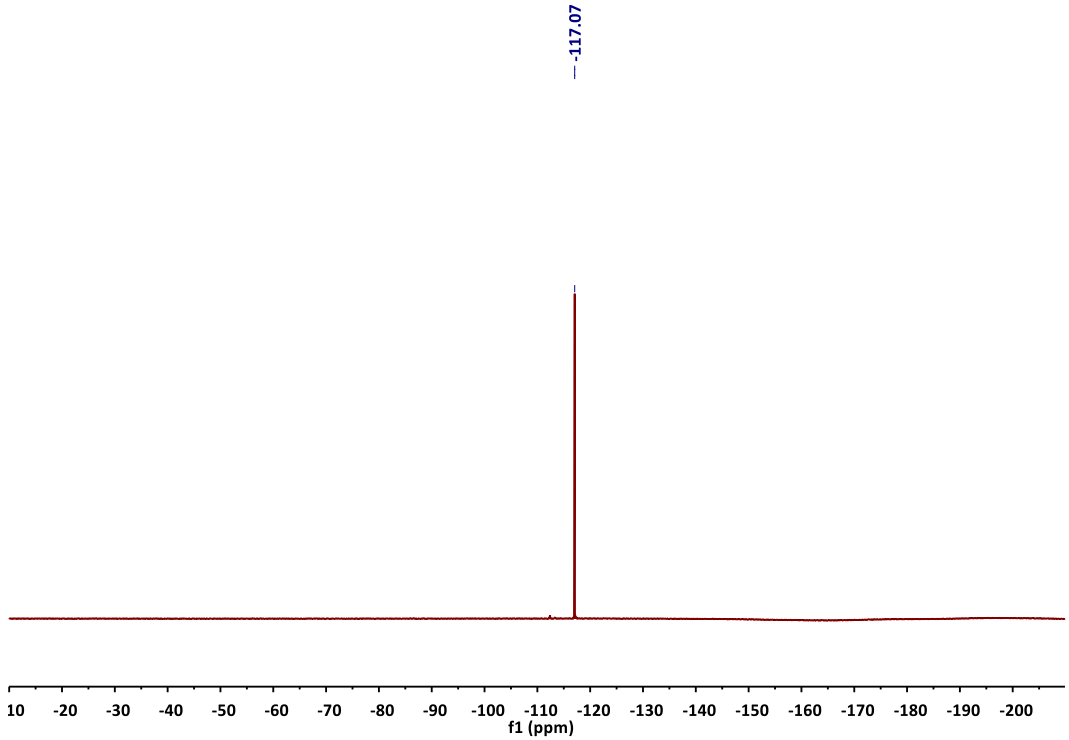

Figure S29. ^{19}F NMR (470 MHz) spectrum of Tetramethyl-N^{1},N^{1},N^{4},N^{4}-tetrakis[3-fluoro-(1,1‘-biphenyl)-4-carboxylate]-1,4-benzene diamine.

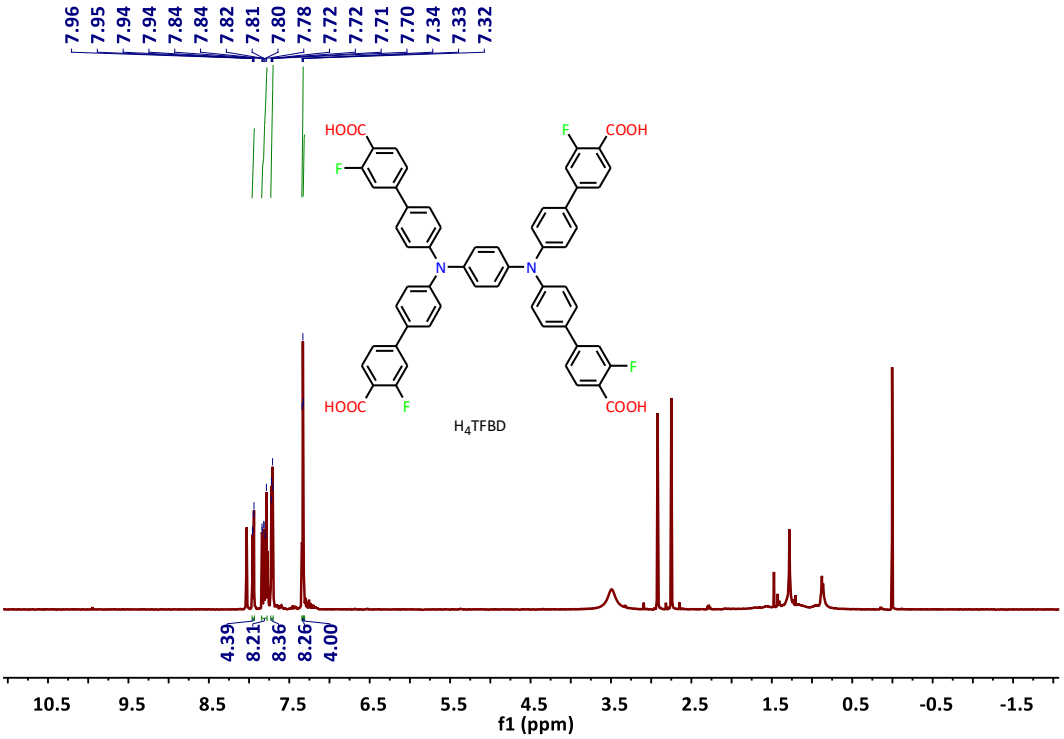

Figure S30. ^{1}H NMR (500 MHz) spectrum of N^{1},N^{1},N^{4},N^{4}-tetrakis[3-fluoro-(1,1'-biphenyl)-4-carboxylic acid]-1,4-benzene diamine.

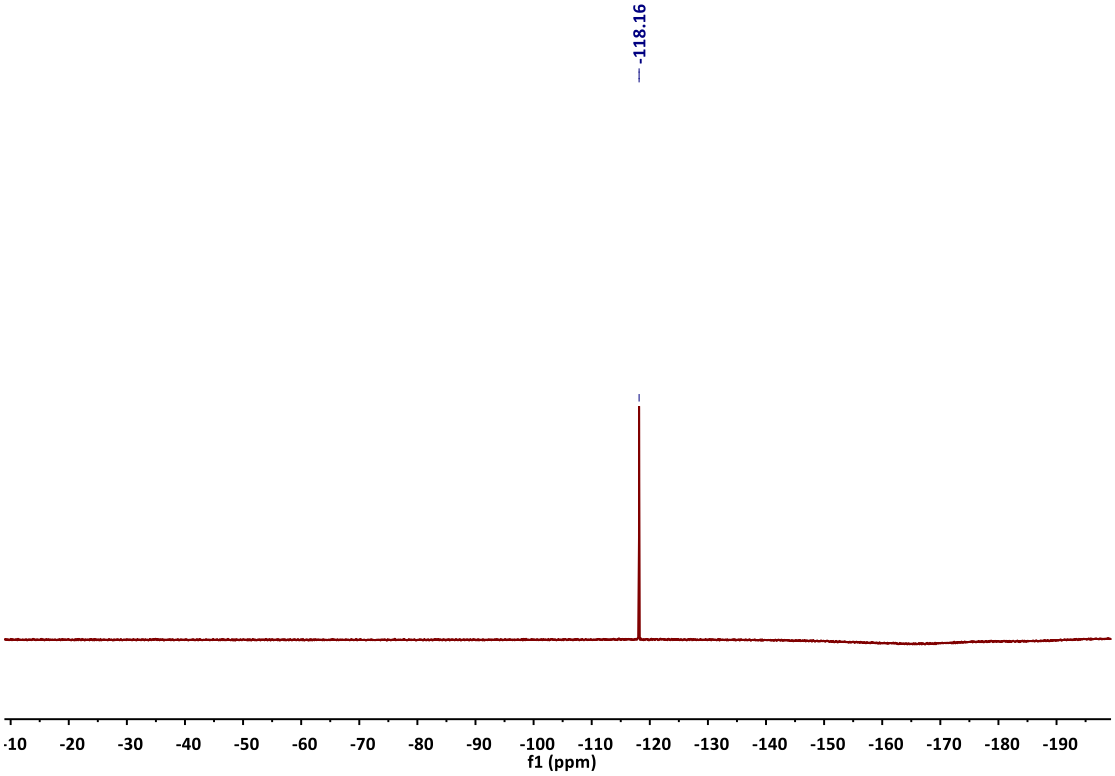

Figure S31. ^{19}F NMR (470 MHz) spectrum of N^{1},N^{1},N^{4},N^{4}-tetrakis[3-fluoro-(1,1'-biphenyl)-4-carboxylic acid]-1,4-benzene diamine.

7. References

S1. L. X. Hou, X. Jing, H. L. Huang and C. Y. Duan, *ACS Appl. Mater. Interfaces*, 2022, **14**, 15307−15316.

S2. D. C. Mayer, A. Manzi, R. Medishetty, B. Winkler, C. Schneider, G. Kieslich, A. Pothig, J. Feldmann and R. A. Fischer, *J. Am. Chem. Soc.*, 2019, **141**, 11594−11602.

S3. L. Li, M. W. Huang, C. Liu, J. C. Xiao, Q. Y. Chen, Y. Guo and Z. G. Zhao, *Org. Lett.*, 2015, **17**, 4714−4717.

S4. Y. Zhu, J. W. Gong and Y. H. Wang, *J. Org. Chem.*, 2017, **82**, 7428−7436.

S5. B. He, Q. J. Pan, Y. Guo, Q. Y. Chen and C. Liu, *Org. Lett.*, 2020, **22**, 6552−6556.

S5. P. Xu, P. L. Rojas and T. Ritter, *J. Am. Chem. Soc.*, 2021, **143**, 5349−5354.

S7. SMART, Data collection software (version 5.629) (Bruker AXS Inc., Madison, WI, 2003).

S8. SAINT, Data reduction software (version 6.45) (Bruker AXS Inc., Madison, WI, 2003).

S9. G. M. Sheldrick, SHELXTL97, Program for crystal structure solution (University of Göttingen: Göttingen, Germany, 1997).

S10. J. M. Taylor, R. K. Mah, I. L. Moudrakovski, C. I. Ratcliffe, R. Vaidhyanathan and G. K. H. Shimizu, *J. Am. Chem. Soc.*, 2010, **132**, 14055−14057.

S11. D. Umeyama, S. Horike, M. Inukai and S. Kitagawa, *J. Am. Chem. Soc.*, 2013, **135**, 11345−11350.

S12. D. Umeyama, S. Horike, M. Inukai, T. Itakura and S. Kitagawa, *J. Am. Chem. Soc.*, 2012, **134**, 12780−12785.

S13. S. Horike, D. Umeyama, M. Inukai, T. Itakura and S. Kitagawa, *J. Am. Chem. Soc.*, 2012, **134**, 7612−7615.

S14. M. Inukai, S. Horike, W. Q. Chen, D. Umeyama, T. Itakurad and S. Kitagawa, *J. Mater. Chem. A,* 2014, **2**, 10404−10409.

S15. M. Inukai, S. Horike, T. Itakura, R. Shinozaki, N. Ogiwara, D. Umeyama, S. Nagarkar, Y. Nishiyama, M. Malon, A. Hayashi, T. Ohhara, R. Kiyanagi and S. Kitagawa, *J. Am. Chem. Soc.*, 2016, **138**, 8505−8511.

S16. H. F. Wang, Y. J. Zhao, Z. C. Shao, W. J. Xu, Q. Wu, X. L. Ding and H. W. Hou, *ACS Appl. Mater. Interfaces*, 2021, **13**, 7485−7497.

S17. G. Q. Shi, H. W. Wang, Q. X Wang and G. Li, *J. Solid State Chem.*, 2022, **307**, 122874.